Wake Formation by Ion Scattering on a Positively Charged Spacecraft

Anders I. Eriksson,* Klaus Gwosch,† and Christopher M. Cully‡
Swedish Institute of Space Physics, Uppsala

Alexander Sjögren§
Embry-Riddle Aeronautical University, Daytona Beach, Florida
(Dated: October 4, 2010)

The wake behind a positively charged spacecraft can grow in size to many times the spacecraft dimensions, if the ion flow kinetic energy is lower than the spacecraft potential times the ion charge, as the ions then undergo Rutherford scattering on the potential. We present analytical and numerical calculations on the resulting enhanced wake, which has received much less attention than wakes behind negative spacraft. Positive potentials mainly appear on photoelectron emitting spacecraft in low density plasmas, for example in the outer magnetoshpere and in interplanetary space. The potentials forming in the wakes in such plasmas are usually small, on the order of a few volts or less, but they can still have a significant impact on precision measurements of plasma parameters and electric fields with instruments on the spacecraft. We derive a simplified semi-analytic test particle model where ions scatter on the spacecraft vacuum field to calculate the ion density in this wake, and compare the results to particle-in-cell (PIC) simulations. The test particle model is several orders of magnitude less demanding on computational resources than the PIC code, though the neglect of impact of wake space charge on ion motion means that the wake size is exaggerated unless the wake size is below the Debye length.

I. INTRODUCTION

In tenuous plasmas, like in the terrestrial magnetosphere outside the inner plasmasphere and in interplanetary space, a sunlit spacecraft normally attains a positive potential V_s with respect to the surrounding plasma, as is well known from theoretical considerations and a wealth of measurements in space[1–6]. The criterion is that the random current to the spacecraft due to thermal motion of the plasma electrons is smaller than the current due to emitted photoelectrons, both evaluated at $V_\mathrm{s} = 0$. In many cases, the ion flow around the spacecraft is supersonic, resulting in the formation of a wake. As the electron thermal speed v_e almost always stays well above the flow speed u, electrons can penetrate the wake which thus is charged negatively. In the outer magnetosphere and the solar wind, typical Debye lengths λ_D are several meters or more, meaning that if the wake dimension is set by the spacecraft, the wake width is only a fraction of a Debye length for most spacecraft. In these circumstances, the potential Φ_w (in volts) due to the wake space charge only reaches a fraction of the electron temperature (in eV), as can be seen by solving Poisson's equation for the electrostatic potential in an infinite slab of width d from which the ions but not the electrons have been removed: for $d \ll \lambda_\mathrm{D}$, the result is that the potential scales as

$$\Phi_w \sim \frac{KT_\mathrm{e}}{e}\left(\frac{d}{\lambda_\mathrm{D}}\right)^2, \tag{1}$$

where KT_e/e is the electron temperature in eV. In consequence, the voltage building up in such a wake is usually modest, but it may still be detectable for a sensitive electric field instrument in e.g. the solar wind, and can thus constitute an unwanted contamination of a measurement of the natural electric field[7].

In the case of plasmas so tenuous that the spacecraft potential (in volts) reaches positive values higher than the ion flow kinetic energy $m_\mathrm{i}u^2/2$ (in eV), the plasma flow around the spacecraft is much more disturbed. In this case, i.e. when

$$eV_\mathrm{s} \gg m_\mathrm{i}u^2/2 \gg KT_\mathrm{i} \tag{2}$$

*Electronic address: Anders.Eriksson@irfu.se
†Now at University of Heidelberg, Germany; Electronic address: Gwosch@stud.uni-heidelberg.de
‡Electronic address: Chris.Cully@irfu.se
§Electronic address: sjogrena@my.erau.edu

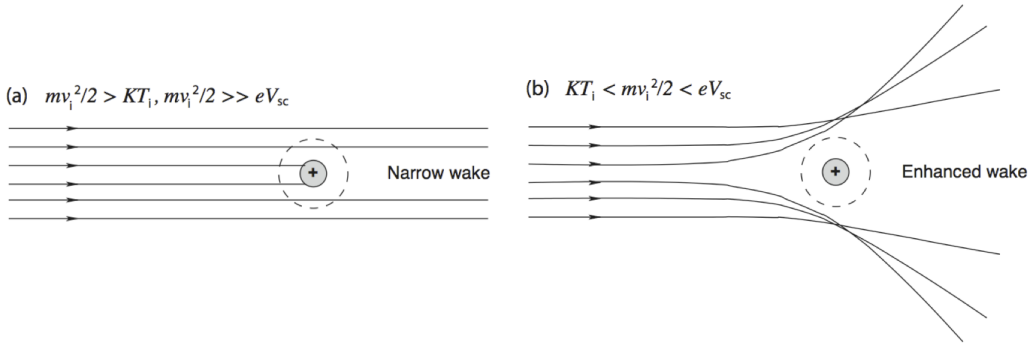

FIG. 1: Illustration of wake formation when the ion energy is above (a) or below (b) the equivalent spacecraft potential.

where T_i is the ion temperature, the ions scatter on the electrostatic potential structure around the spacecraft rather than reaching the solid obstacle itself. As illustrated in Figure 1, the wake size is therefore very much enhanced, and with it also the wake potential. Such an enhanced wake has been observed with the Cluster satellites in the tenuous plasma of the Earth's geomagnetic tail due to the polar wind flow[8, 9], and its properties were studied by numerical simulations[10]. Based on that understanding, it was possible to turn the wake detection into a method for actually measuring the flow velocity of the polar wind[11, 12], which is otherwise quite elusive[13] as it cannot reach ion detectors on a spacecraft charged positively by photoemission because of relation (2), unless elaborate measures are taken to artificially control the spacecraft potential[9, 14, 15].

In this study, we explore the possibilities of a simple test particle model to provide analytical results on the formation of an enhanced ion wake, neglecting any plasma interactions. The model is developed in Section II and compared to results of previously published particle-in-cell simulations in Section III.

II. ANALYTICAL MODEL

A. Model and assumptions

To get an analytically tractable problem, we will assume a spherical spacecraft with conducting surfaces at potential V_s. While most spacecraft bodies can reasonably be approximated as spheres, the long wire booms used for measuring electric fields on scientific spacecraft complicates the situation[16]. Our results must therefore be applied to such spacecraft with some caution.

For the tenuous plasmas we consider, we assume that space charge effects can be neglected, so that the electrostatic potential Φ at a distance r from the centre of a spherical spacecraft of radius R is given by the Coulomb potential

$$\Phi(r) = V_\mathrm{s}\frac{R}{r} = \frac{\alpha}{r} \tag{3}$$

where we introduced $\alpha = V_\mathrm{s}R$. This should be a good description for Debye lengths much above the spacecraft radius. The photoelectron sheath forming around a spacecraft can give a large shielding in tenuous plasmas, but for spacecraft potentials (in volts) much above the typical photoelectron energy T_f (in eV), the photoelectrons cannot escape far from the spacecraft and their shielding effect is thus small. As T_f is a few eV[17], the effect of photoelectron shielding should be negligible for spacecraft potentials in the tens of volts range.

To find the wake structure, we will consider ion scattering on the spacecraft Coulomb potential field. This means that we ignore any effects of space charge forming in the wake itself. This is justified if the potential Φ_w due to this space charge is much smaller than the spacecraft potential, which will be the case if the wake does not reach Debye length scale, or if T_e (in eV) is much below the spacecraft potential (in volts). The applicability of these conditions may vary. For the magnetotail conditions of chief interest to us, the latter condition is guaranteed by (2) if $T_\mathrm{e} \sim T_\mathrm{i}$. For wakes in the solar wind, the second condition will be violated, but instead the first one will typically be satisfied[7].

With these assumptions, we embark on the following programme to establish the wake structure:

1. Establish ion trajectories in the spacecraft Coulomb field, and use this to find the initial velocity at infinity for an ion with velocity $\mathbf{v}$ at position $\mathbf{r}$ (Section II B).

2. Use Lioville's theorem to find the distribution function at $\mathbf{r}$ in terms of the distibution at infinity (Section II C).

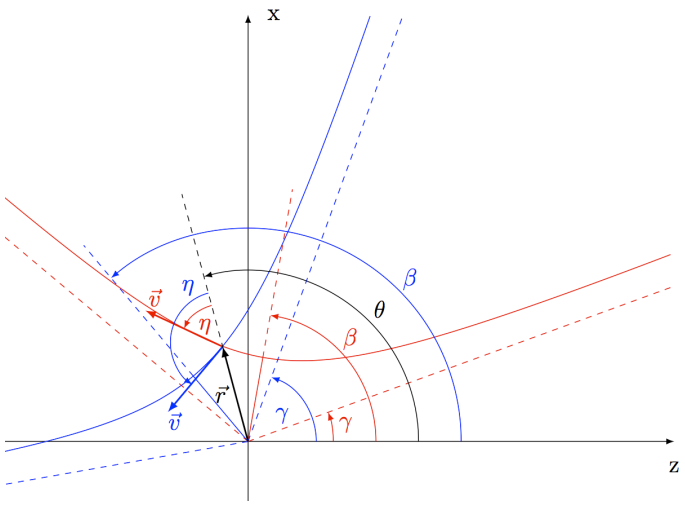

FIG. 2: Ion trajectories and angles for describing them. Blue/red indicates that the reference point (r, θ) is located before/after the periapsis on the trajectory.

3. Integrate to find the ion density at **r** (Section II D).

B. Ion trajectories

The motion of an ion in a Coulomb field can be treated in the same way as the Kepler problem for Newtonian gravitational attraction, and the trajectory can be found by textbook procedures [18, p. 35]. For a repelling potential, the result is a hyperbola, described in polar coordinates by

$$\frac{p}{r} = \epsilon \cos(\theta - \beta) - 1, \tag{4}$$

where

$$p = \frac{l^2}{m\alpha} \tag{5}$$

is the semilatus rectum,

$$\epsilon = \sqrt{1 + \frac{2El^2}{m\alpha^2}} \tag{6}$$

the eccentricity, l the angular momentum, β the direction of the periapsis (Figure 2) and E the conserved total energy

$$E = \frac{1}{2}mv^2 + \frac{\alpha}{r} = \frac{1}{2}mv_0^2. \tag{7}$$

We can use these relations to find the initial velocity $\mathbf{v}_0$ (at infinity) of a particle with velocity $\mathbf{v}$ at position $\mathbf{r}$. The magnitude v_0 of this velocity follows immediately from energy conservation, but the direction requires some more analysis. As the motion is in a plane, the problem is two-dimensional. The direction γ of the incoming asymptote is given by letting $r \to \infty$ in (4):

$$\cos(\gamma - \beta) = \frac{1}{\epsilon}. \tag{8}$$

Introducing

$$\delta = \arccos\left(\frac{1}{\epsilon}\right) \tag{9}$$

and

$$\zeta = \arccos\left(\frac{1}{\epsilon}\left[\frac{p}{r}+1\right]\right) \tag{10}$$

we use (4) and (8) to get

$$\cos(\theta-\beta) = \cos(\gamma-\beta)\cos\zeta = \cos\delta\,. \tag{11}$$

We can now solve for the incoming asymptote γ, properly caring for the signs of the inverse cosines. In the range $0 \le \theta \le \pi$, we have to differ between the cases of incoming and outgoing particles, to be sure we map particles back to infinity along the incoming track. These cases are illustrated in Figure 2, in which we find that

$$\gamma = \begin{cases} \theta - \zeta - \delta & \text{for } 0 \le \eta \le \frac{\pi}{2} \\ \theta + \zeta - \delta & \text{for } \frac{\pi}{2} \le \eta \le \pi \end{cases} \tag{12}$$

where η is the angle of the velocity to the radius vector. Combining with

$$v_0^2 = v^2 + \frac{2\,\alpha}{m\,r}, \tag{13}$$

from the conservation of total energy (7), we thus have both the magnitude and direction of the initial velocity at infinity of any ion at $\mathbf{r}$.

C. Distribution function

Assuming a homogeneous plasma, with an ion population isotropic in its own rest frame, the ion distribution function in spacecraft-centred position-velocity phase space far from the spacecraft can be written

$$\lim_{r\to\infty} f(\mathbf{r},\mathbf{v}_0) = f_0\left(\left[\mathbf{v}_0-\mathbf{u}\right]^2\right) \tag{14}$$

and we can choose coordinates such that $\mathbf{u}$, the plasma flow velocity in the spacecraft frame, is along the z-axis. The wake then is rotationally symmetric around the z-axis, so we only need to find the distribution function in the xz plane.

By Liouville's theorem [18, p. 147], the distribution function is constant along particle trajectories, so we can find the distribution function at the point $\mathbf{r}$ from f_0 by tracking particles back to infinity along their incoming path as determined in Section II B. We assume a velocity $\mathbf{v}$ at position $\mathbf{r}$ and describe the velocity by local coordinates (whose Cartesian components we denote by $'$) at $\mathbf{r}$ such that the z'-axis is $\mathbf{r}/r$. We can describe the velocity direction in this plane by the polar angle η introduced in (12) and Figure 2.

While we only need to find the distribution function in a plane, and the particle trajectories studied in Section II B are also planar, these planes do not need to coincide. To describe the velocity we therefore also need an azimuthal angle ω around the z' axis, measured from the x' axis. Thus (v,η,ω) can be used as a spherical coordinate system in velocity space, suitable for describing the distribution at position $\mathbf{r}$. As an ion trajectory is in a plane containing the spacecraft, the problem is symmetric around $\mathbf{r}$, so we can calculate the incoming asymptote for $\omega = 0$ and rotate it by ω around $\mathbf{r}$ to get the correct asymptote. The incoming asymptote for $\omega = 0$ is given by (12), with the parameters p and e derived from $\mathbf{r}$ and $\mathbf{v}$ by use of (13) and

$$l^2 = m_\mathrm{i}^2\,(\mathbf{r}\times\mathbf{v})^2 = m_\mathrm{i}^2\,r^2\,v^2\,\sin^2\eta\,. \tag{15}$$

For $\omega = 0$, the initial velocity is

$$\mathbf{v}_0' = -v_0\,\mathbf{\Gamma}' \tag{16}$$

where

$$\mathbf{\Gamma}' = \begin{pmatrix} \sin\gamma \\ 0 \\ \cos\gamma \end{pmatrix}. \tag{17}$$

We can use a rotation matrix R to rotate $\mathbf{v}_0'$ around $\hat{\mathbf{r}} = (x',y',z')$ (normalized) by an angle ω to get the initial velocity $\mathbf{v}_0$. The general form of this rotation matrix is

$$\mathrm{R} = \begin{pmatrix} \cos\omega + x'^2(1-\cos\omega) & x'y'(1-\cos\omega) - z'\sin\omega & x'z'(1-\cos\omega) + y'\sin\omega \\ y'x'(1-\cos\omega) + z'\sin\omega & \cos\omega + y'^2(1-\cos\omega) & y'z'(1-\cos\omega) - x'\sin\omega \\ z'x'(1-\cos\omega) - y''\sin\omega & z'y'(1-\cos\omega) + x'\sin\omega & \cos\omega + z'^2(1-\cos\omega) \end{pmatrix} \tag{18}$$

and the initial velocity is then

$$\mathbf{v}_0 = -v_0\,\mathrm{R}\,\mathbf{\Gamma}'\,. \tag{19}$$

The term $(\mathbf{v}_0 - \mathbf{u})^2$ in the distribution function can now be written as

$$(\mathbf{v}_0 - \mathbf{u})^2 = v_0^2 + u^2 - 2\,\mathbf{v}_0\cdot\mathbf{u} \;= v_0^2 + u^2 + 2\,v_0\,u\;(\mathrm{R}\,\mathbf{\Gamma}')_z \tag{20}$$

where

$$(\mathrm{R}\,\mathbf{\Gamma}')_z = [z'x'(1-\cos\omega)]\sin\gamma \;+ \left[\cos\omega + z'^2(1-\cos\omega)\right]\cos\gamma \tag{21}$$

by (17) and (18). We have here restricted ourselves to the xz plane, which as noted above causes no loss of generality because of the symmetry of the problem.

D. Density integration

Having established the distribution function, the density follows by integration over velocity space:

$$n(\mathbf{r}) = \int f(\mathbf{r},\mathbf{v})\,\mathrm{d}^3v \tag{22}$$

To actually calculate this integral, we must specify the functional form of the distribution function. Far away from the spacecraft, we assume a homogeneous Maxwellian ion population of density n_0, temperature T_i and drift velocity $\mathbf{u}$. The distribution function at infinity then is

$$f_0(\mathbf{v}_0) = A\,\exp\left(-\frac{(\mathbf{v}_0-\mathbf{u})^2}{v_\mathrm{t}^2}\right) \tag{23}$$

where $v_\mathrm{t} = \sqrt{\frac{2KT}{m_\mathrm{i}}}$ is the ion thermal speed and

$$A = n_0\left(v_\mathrm{t}^2\,\pi\right)^{-3/2}\,. \tag{24}$$

The density in the xz-plane at (r,θ) is given by

$$n(r,\theta) = A\int \exp\left(-\frac{u^2 + v_0^2 + 2\,u\,v_0\;(\mathrm{R}\,\mathbf{\Gamma}')_z}{v_\mathrm{t}^2}\right)\,\mathrm{d}^3v \tag{25}$$

or, in the spherical coordinates (v,η,ω) introduced in Section II C and with use of (13),

$$n(r,\theta) = A\exp\left(-\frac{u^2+\frac{2\,\alpha}{m\,r}}{v_\mathrm{t}^2}\right)\int_0^{2\pi}\int_0^{\pi}\int_0^{\infty}\exp\left(-\frac{v^2}{v_\mathrm{t}^2}\right)\exp\left(-\frac{2\,u\sqrt{v^2+\frac{2\,\alpha}{m\,r}}\;(\mathrm{R}\,\mathbf{\Gamma}')_z}{v_\mathrm{t}^2}\right)v^2\mathrm{d}v\,\sin\eta\,\mathrm{d}\eta\,\mathrm{d}\omega\,. \tag{26}$$

The integrand depends on ω only through the $\cos\omega$ term in $\mathrm{R}\,\mathbf{\Gamma}'$. For the ω integration, we may thus use the mathematical identity [19, Eqn. 9.6.16]

$$\int_0^{2\pi}\exp(x\cos\omega)\,\mathrm{d}\omega = 2\pi I_0(x)\;, \tag{27}$$

where I_0 is a modified Bessel function, to get

$$n(r,\theta) = 2\pi A\exp\left(-\frac{u^2+\frac{2\,\alpha}{m\,r}}{v_\mathrm{t}^2}\right)\int_0^{\infty}\int_0^{\pi}\exp\left(-\mu\,\cos\theta\,\cos(\gamma-\theta)\right)I_0\left(\mu\,\sin\theta\,\sin(\gamma-\theta)\right)\sin\eta\,\mathrm{d}\eta\,\exp\left(-\frac{v^2}{v_\mathrm{t}^2}\right)v^2\mathrm{d}v\,, \tag{28}$$

where

$$\mu = \frac{2\,u\,\sqrt{v^2 + \frac{2\,\alpha}{m\,r}}}{v_{\rm t}^2} \tag{29}$$

and due care should be taken with the sign of γ (Eqn. 12). While the integrand in (28) depends non-trivially on η through the angular momentum (Eqns. 6, 9, 10 and 15), it lends itself well for numerical integration. We use a simple Monte Carlo scheme, equivalent to summing the contributions from a large number of particles picked from a random distribution uniform in η and in the interval $u - \nu\,v_{\rm t} < v < u + \nu\,v_{\rm t}$, where we mostly used $\nu = 6$, checking results by reference simulations with $\nu = 10$. While not in any way optimized, this method can evaluate the density in a few hundred points around the spacecraft, evaluating the trajectories of some 10^5 particles at each position, in a few minutes on a standard personal computer, which is sufficient for our needs.

III. COMPARISON TO PIC RESULTS

To test the method, we compare the ion density obtained from Equation (28) to previous results from particle-in-cell simulations. The case of a flowing hydrogen plasma $n_0 = 0.2$ cm^{-3}, $T_{\rm e} = T_{\rm i} = 2$ eV, $u = 43.77$ km/s (proton ram energy 10 eV) and $V_{\rm s} = 35$ V have been simulated with the two PIC codes PicUp3D [10] and SPIS [20], so we chose the same parameters. Following [10], we take a sphere of radius 1.4 m to describe the approximately cylindrical satellites (height 1.5 m, radius 1.45 m). The results can be seen in Figures 3 and 4. The underlying color plots show the ion density derived from PIC simulations, while the solid black curves represent some isodensity contours from the Monte Carlo simulation of (28). We can note that while the general picture of the wake is quite similar, the wake produced in our Monte Carlo method is significantly larger than what the PIC codes say. Upstream of the spacecraft, all three codes give similar results, but the wake fills in much more slowly in our study than in the PicUp3D and SPIS simulations. On the other hand, the two PIC codes agree well with each other. As these two codes are quite different, with PicUp3D using a uniform Cartesian grid [21] and SPIS an unstructured mesh [22], this points to effects of the limitations of the present method rather than to any problem with the PIC simulations.

The three most prominent limitations with the present method are: (i) by using a vacuum expression for the potential, we overestimate the number of particles energy conservation forbids to reach a particular point; (ii) in a shielding-modified spacecraft potential field, the ions will not follow hyperbolic trajectories, thus invalidating the basic assumptions behind the integrand in (28); and (iii) we neglect the increased filling-in of the wake due to impact of the wake space charge on the ion flow. While (ii) and (iii) cannot be handled within the present approach, we can approximate the effects of (i) by including a Debye shielding term in (29) and in the first exponential in (28), i.e. by in these positions substituting

$$\frac{\alpha}{r} \longrightarrow \frac{\alpha}{r}\,\exp\left(\frac{R-r}{\lambda_{\rm D}}\right) \tag{30}$$

where R is the spacecraft radius and $\lambda_{\rm D}$ the Debye length. This means that while we still assume hyperbolic orbits, but allow more ions to reach closer to the satellite body as merited by the decrease in their potential energy introduced by the shielding. As known from basic plasma physics, the exponential Debye shielding in (30) originates from the linearization of the Boltzmann distribution, and thus assumes that the local value of the potential varies is proportional to the electron density. Without linearization, the electron density in space around a positive sphere varies less steeply than so [23], and we may therefore assume that the density we derive from (28) when using (30) is an upper limit with regard to this particular effect.

The result of using this modified potential in the energy expressions can be seen as dashed curves in Figures 3 and 4 (green in the first case, red in the second, to enhance contrast). We find that while the shielding indeed decreases the wake slightly, the difference to the $1/r$ case is still small. This tells us that the difference between our Monte Carlo result and the PIC simulations cannot be explained by this effect, and should thus rather be due to (ii) or (iii) above. Inspection of Figures 3 and 4 shows that while our isodensity contours agree reasonably well in shape with the PIC derived contours upstream and transverse from the spacecraft body, the PIC contours curve to cut off the wake much closer to the spacecraft than do our results. This suggests that (iii), the enhanced filling in of the wake, is the main reason for the observed discrepancy. This is very reasonable for the present parameters, as the Debye length (defined on electrons only) is close to 10 m. The size of the wake we find in the Monte Carlo simulation is something like 50 m in the smallest direction, and thus we would need Debye lengths of this order in order for our neglect of space charge would be fully justified.

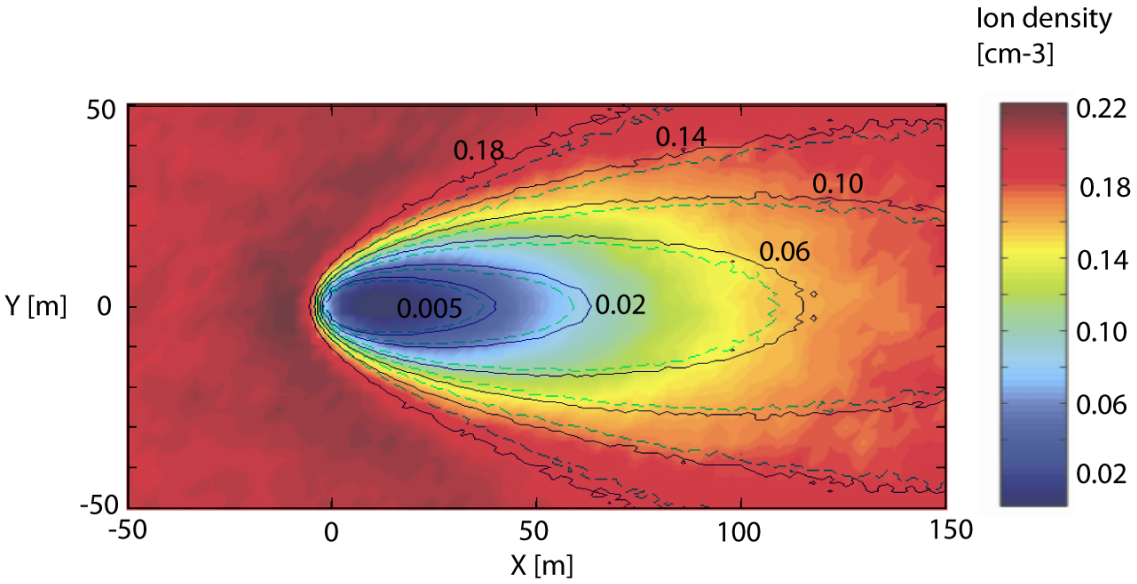

FIG. 3: Comparison to PIC results. Color plot: Simulation using PicUp3D by [10, color version of Fig. 2a]. Solid black curves: Result of Monte Carlo simulation. Dashed green curves: Result of Monte Carlo simulation, with Debye shielding adjustment for the potential energy. The contours have been computed for one half plane only and mirrored in the X axis, as allowed by the symmetry of the situation.

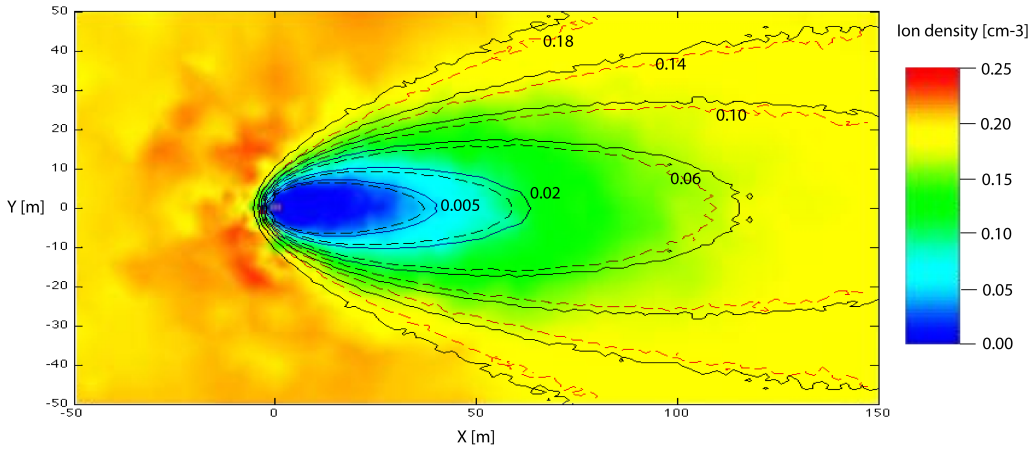

FIG. 4: Comparison to PIC results. Color plot: Simulation using SPIS 3.1 by [20, Fig. 10.1]. Solid black curves: Result of Monte Carlo simulation. Dashed red curves: Result of Monte Carlo simulation, with Debye shielding adjustment for the potential energy. The contours have been computed for one half plane only and mirrored in the X axis, as allowed by the symmetry of the situation.

IV. CONCLUSION

We have here presented a simplified approach to wake formation behind a positively charged spacecraft, based on the analytical calculation of particle trajectories in a $1/r$ potential. The method offers insight into the process of wake formation behind a highly positive spacecraft, and provides a tool for understanding and modeling of such phenomena. However, all plasma interactions are turned off in the model, which thus is expected to well reproduce the ion density only when the Debye length is large compared to the width of the wake, so that the wake field stays weak and cannot much influence ion motion. In case this is not satisfied, plasma effects become important, and the present method will predict a too wide and deep ion wake, as we found when comparing to previous results from two PIC codes. While the method offers great computational advantages as compared to full PIC simulations, its numerical results must be interpreted with caution, and it cannot replace full PIC simulations in the general case. However, in some situations where the ion ram flow energy is much higher than the potentials forming in the wake, which are of the order of or smaller than KT_e/e, the method should provide good results on the effect of a highly positive spacecraft potential, $V_s \gg KT_e/e$, on the ion wake. This happens regularly for spacecraft in the solar wind [7], for which the method results could be compared to observations.

Acknowledgments

AS acknowledges support from the US Air Force Research Laboratory for presenting this work at SCTC-11.

[1] Y. L. Alpert, A. V. Gurevich, and L. P. Pitaevskii, *Space Physics with Artificial Satellites* (Consultants Bureau, 1965).
[2] E. C. Whipple, Ph.D. thesis, George Washington University (1965).
[3] P.-A. Lindqvist, in *Proc. of the 17th ESLAB Symp. on Spacecraft/Plasma Interactions and their Influence on Field and Particle Measurements, Noordwijk, The Netherlands, ESA SP-198* (European Space Agency, 1983), pp. 25–33.
[4] A. Pedersen, Ann. Geophysicae **13**, 118 (1995).
[5] H. Laakso, J. Atm. Solar-Terr. Phys. **64**, 1735 (2002).
[6] B. Thiebault, A. Hilgers, A. Masson, C. P. Escoubet, and H. Laakso, IEEE Proc. Plasma Sci. **34**, 2078 (2006).
[7] A. I. Eriksson, Y. Khotyaintsev, and P.-A. Lindqvist, in *Proceedings of the 10th Spacecraft Charging Technology Conference (SCTC-10)* (2007).
[8] A. I. Eriksson, M. André, B. Klecker, H. Laakso, P.-A. Lindqvist, F. Mozer, G. Paschmann, A. Pedersen, J. Quinn, R. Torbert, et al., Ann. Geophysicae **24**, 275 (2006).
[9] E. Engwall, A. I. Eriksson, M. André, I. Dandouras, G. Paschmann, J. Quinn, and K. Torkar, Geophys. Res. Lett. **33**, L06110, doi:10.1029/2005GL025179 (2006).
[10] E. Engwall, A. I. Eriksson, and J. Forest, Phys. Plasmas **13**, 062904 (2006).
[11] E. Engwall, A. I. Eriksson, C. M. Cully, M. André, R. Torbert, and H. Vaith, Nature Geoscience **2**, 24 (2009).
[12] E. Engwall, A. I. Eriksson, C. M. Cully, M. André, P. A. Puhl-Quinn, H. Vaith, and R. Torbert, Annales Geophysicae **27**, 3185 (2009), ISSN 0992-7689, URL `http://www.ann-geophys.net/27/3185/2009/`.
[13] R. C. Olsen, J. Geophys. Res. **87**, 3481 (1982).
[14] T. E. Moore, C. R. Chappell, M. O. Chandler, P. D. Craven, B. L. Giles, C. J. Pollock, J. L. Burch, D. T. Young, J. Hunter Waite, J. E. Nordholt, et al., Science **277**, 349 (1997).
[15] Y.-J. Su, J. L. Horwitz, T. E. Moore, L. Giles, M. O. Chandler, P. D. Craven, M. Hirahara, and C. J. Pollock, J. Geophys. Res. **103**, 29305 (1998).
[16] C. Cully, R. E. Ergun, and A. I. Eriksson, J. Geophys. Res. **112**, A09211, doi:10.1029/2007JA012269 (2007).
[17] R. J. L. Grard, J. Geophys. Res. **78**, 2885 (1973).
[18] L. D. Landau and E. M. Lifshitz, *Mechanics, Course of Theoretical Physics vol 1* (Pergamon, 1969).
[19] M. Abramowitz and I. A. Stegun, *Handbook of mathematical functions with formulas, graphs, and mathematical tables* (Dover Books, 1965).
[20] R. Prakash, Tech. Rep., student internship report, Swedish Institute of Space Physics, Uppsala (2007).
[21] J. Forest, A. Hilgers, B. Thiebault, L. Eliasson, J.-J. Berthelier, and H. D. Feraudy, IEEE Proc. Plasma Sci. **34**, 2103 (2006).
[22] J.-F. Roussel, F. Rogier, G. Dufour, J.-C. Mateo-Velez, J. Forest, A. Hilgers, D. Rodgers, L. Girard, and D. Payan, IEEE Transactions on Plasma Science **36**, 2360 (2008).
[23] J. G. Laframboise and L. W. Parker, Physics of Fluids **16**, 629 (1973), URL `http://link.aip.org/link/?PFL/16/629/1`.
[24] E. Engwall, *Numerical Studies of Spacecraft-Plasma Interaction: Simulations of Wake Effects on the Cluster Electric Field Instrument EFW*, IRF Scientific Report 284 (Swedish Institute of Space Physics, Uppsala (http://www.irf.se/Publications/IRFreport284.pdf), 2004).